A 512×96-Pixel 50fps Line-Scanning Direct Time-of-Flight LiDAR Achieving Fog/Rain Removal and 2× Vertical Super-Resolution

Chaorui Zou, Yan Zhu, Chi-Hang Chan, Rui P. Martins, and Minglei Zhang
State-Key Laboratory of Analog and Mixed-Signal VLSI, University of Macau, Macau, China
Email: mlzhang@um.edu.mo

***Abstract*—This paper introduces a direct time-of-flight (dToF) LiDAR that embeds fog/rain extraction capabilities within its analog front-end (AFE). A pulse extraction (PE) transimpedance amplifier (TIA) differentiates the actual ToF signal from interference caused by fog/rain, together with a dual peak accumulation (DPA) algorithm, extending the 10%-reflectivity detection distance from 90m to 170m in foggy conditions with 120m of visibility. Additionally, the LiDAR employs a pixel-multiplexing (PM) technique to achieve 2× super-resolution in the vertical; thereby, 48× AFEs operating in line-scanning mode can provide a depth image resolution of 512×96 pixels at 50 frames per second (fps). Furthermore, self-charged background-light-induced current compensation, noise cancellation, and event-driven integration enhance the TIA performance, facilitating greater energy efficiency and extended detection capabilities.**

***Keywords*—LiDAR, 3D ranging systems, direct time-of-flight (dToF), fog/rain removal, and super-resolution**

I. Introduction

LiDAR plays a vital role in Level 3 autonomous driving and beyond, offering better anti-interference capabilities compared to pure vision solutions. Even so, it still encounters constraints, particularly in terms of detection distance and accuracy in adverse weather conditions, such as fog and rain. As indicated in Fig. 1, laser pulses reflected from targets are weakened in fog and rain. In addition, strong reflections caused by these weather conditions can be misinterpreted as time-of-flight (ToF) measurements, as they overlap with reflections from actual targets, which degrades the quality of depth imaging. One potential solution to mitigate these interferences is to use an analog-to-digital converter to digitize all reflected echoes from both the interferences and the targets [1]. Post-processing can then identify targets amidst the fog/rain interference by leveraging data from additional sensors or employing deep learning techniques [2]. However, this approach necessitates complex processors and precise 2D/3D waveform readouts, thereby deteriorating latency and energy efficiency. Moreover, high image resolution is crucial for accurate depth perception, especially when detecting pedestrians at distances beyond 100 meters. However, scanning LiDAR [3] faces intrinsic constraints on channel count and frames per second (fps) for a given image resolution. While increasing the number of channels can improve image resolution, it brings significant area overhead. Alternatively, performing more frequent scans can enhance depth image resolution, but this typically decreases the fps. This paper demonstrates a line-scanning direct-ToF LiDAR that incorporates fog/rain extraction within the analog front-end (AFE) and supports 2× vertical-pixel super-resolution. The key innovations of the prototype LiDAR include: 1) a pulse extraction (PE) transimpedance amplifier (TIA) that

This work was supported by NSFC (File no. 624B2001) and Macau FDCT (File no. 0129/2024/AMJ, 0137/2024/RIB2, and 0001/2025/NRP).

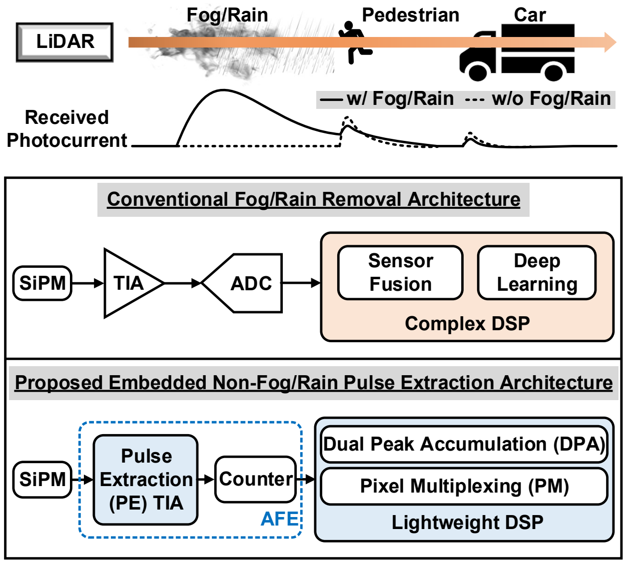

Fig. 1. Reflected echoes in adverse weather conditions; comparison between conventional and proposed fog/rain removal architectures.

separates the target echo pulse from the photocurrent disturbed by adverse weather, facilitating fog/rain removal alongside a lightweight dual peak accumulation (DPA) algorithm; 2) a pixel multiplexing (PM) technique that doubles vertical pixel resolution without adding extra AFE channels; and 3) a self-charged I_{dc} compensation, noise cancellation, and event-driven fine integrating clock generation that enhance the readout performance of the proposed PE-TIA.

II. LiDAR AFE Implementations and Algorithms

Fig. 2 presents the architecture of the line-scanning LiDAR, highlighting two key features: fog/rain removal and super-resolution. It includes 48× AFEs and a lightweight digital signal processor (DSP). Each AFE consists of a PE-TIA that differentiates between the overlapping photocurrent pulses caused by fog/rain and those generated by actual targets. Additionally, each AFE is equipped with two counters that respectively record the ToF and the intensity of the separated pulse echoes. The PE-based AFE enables the subsequent DPA algorithm to accurately identify target echoes despite interference from fog/rain, thereby improving LiDAR performance under adverse weather scenarios. Additionally, by leveraging multiple echoes from each AFE channel within a single LiDAR measurement, the PM technique supports mapping from one AFE channel to two image pixels, achieving 2× super-resolution without incurring additional AFE hardware costs. As a result, the 1D line-scanning LiDAR can deliver a vertical pixel resolution of 96 using only 48× PE-TIAs, thus enhancing imaging quality. Compared to [4] and [5], the pixel efficiency of each

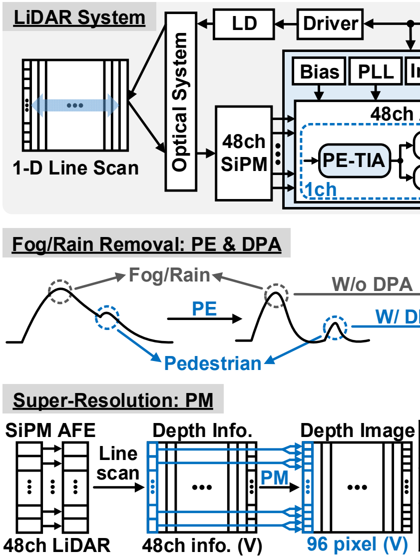

	This work	[4]	[5]
Channel	48	40	20
Equiv. pixel/ch	2	1	0.5

Fig. 2. Line-scanning LiDAR architecture with fog/rain removal and super-resolution techniques.

SiPM/AFE channel increases by 2× and 4×, respectively, resulting in either higher fps or enhanced pixel resolution.

A. Pulse-Extraction TIA

Fig. 3 shows the PE-TIA, which integrates a PE stage into the conventional current-integrating (CI) TIA [6]. The current-mirror-based PE stage subtracts a time-delayed photocurrent duplicate (I_{Z1}) from the original photocurrent (I_Z), which converts the absolute current to a relative current. This process allows the superimposed current pulse to be separated into two distinct pulses, making it easier for the DPA to interpret their digital representations of ToF and intensity for fog/rain removal. The PE process can benefit from a low-noise TIA. Since the regulated common-gate (RCG) stage dominates the noise power of the TIA and constrains the detection range, a noise cancellation branch ($M_{3/4/5}$) [7] is applied to improve its noise performance. This cancellation branch amplifies the noise at node X and counteracts the output noise of the RCG stage at node Y in the opposite direction, which helps to reduce the TIA's total input-referred noise density by 36% while improving its ability to detect weak photocurrents. Furthermore, enhancing robustness against background light-induced I_{dc} necessitates more precise I_{dc} compensation [6]. To address this, a self-charged current mirror (M_1) is proposed, which is shared during the I_{dc} recording and cancellation phases, reducing the 1σ residual I_{dc} from 8.3μA to just 0.13μA while conserving significant power and silicon area.

The weak current (ΔI_Z) after the PE is first amplified by a current amplifier and then integrated through a CI stage. The CI operation enables a straightforward counter to record ToFs while simultaneously acquiring intensity, assisting the DPA in eliminating the photocurrent pulse caused by adverse weather conditions. However, a significant challenge arises due to the need for a high-speed integrating clock to improve time resolution. In Fig. 4, the proposed event-driven fine clock generation mechanism achieves a time resolution of 100ps using a 1GHz PLL, representing a 10× reduction in PLL frequency compared to [6]. The 1GHz clock (CLK_C) initiates the integration process. Two complementary paths halve the time resolution, with switching occurring between

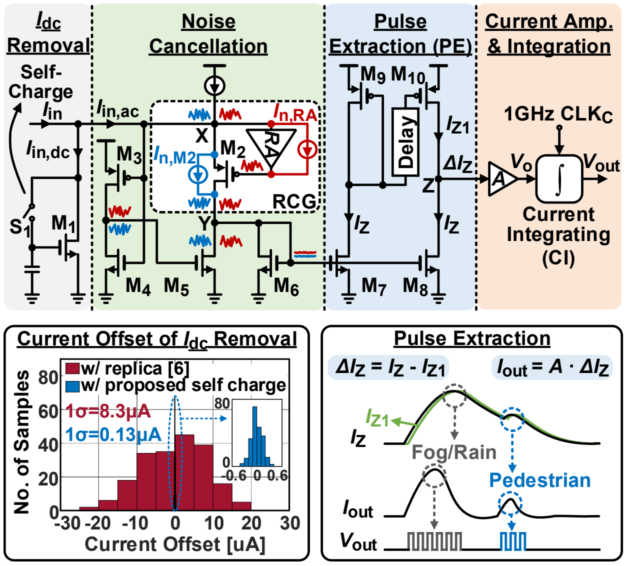

Fig. 3. Implementation of pulse extraction (PE) TIA, highlighting the current offset of I_{dc} removal and pulse extraction mechanism.

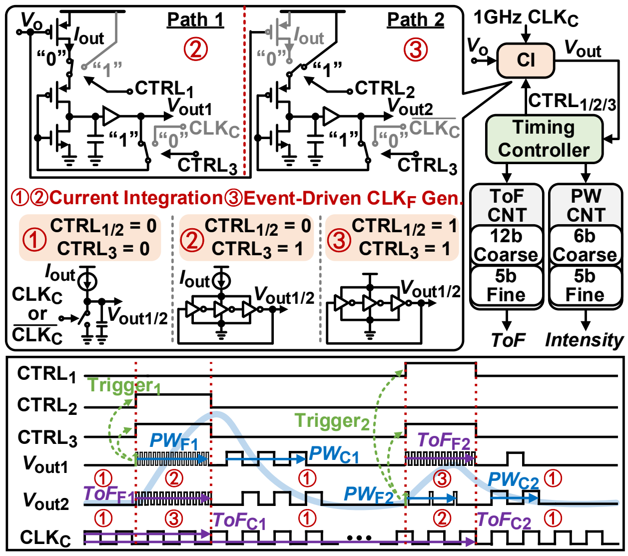

Fig. 4. Implementation and operation of the current integrating (CI) stage in the PE-TIA with a detailed timing diagram.

CI mode and fine clock generation mode, controlled by event-driven outputs ($CTRL_{1/2/3}$) from a timing controller. The path that detects a pulse-echo event acts as a current-controlled ring oscillator (RO), allowing the input intensity to be represented by the number of pulses produced, thus providing fine intensity information. This path also triggers the other path for fine clock generation, which operates independently of the integrating current to prevent variations in the integrating current from affecting time resolution. The PE-TIA attains a transimpedance gain of 118dBΩ, enabling long-range detection. During detection, the ToF (from fine clock generation mode) and intensity (from CI mode) are mixed in V_{out1} and V_{out2}. The timing controller monitors the PE-TIA outputs ($V_{out1/out2}$) and separates the ToF and intensity, enabling the counters to record them separately. Moreover, the ToF is recorded using a 12b 1ns-step coarse counter, alongside a 5b 100ps-step fine counter. The intensity (pulse width) is captured using a 6b 1ns-step coarse counter and a 5b fine counter with an adaptive step size.

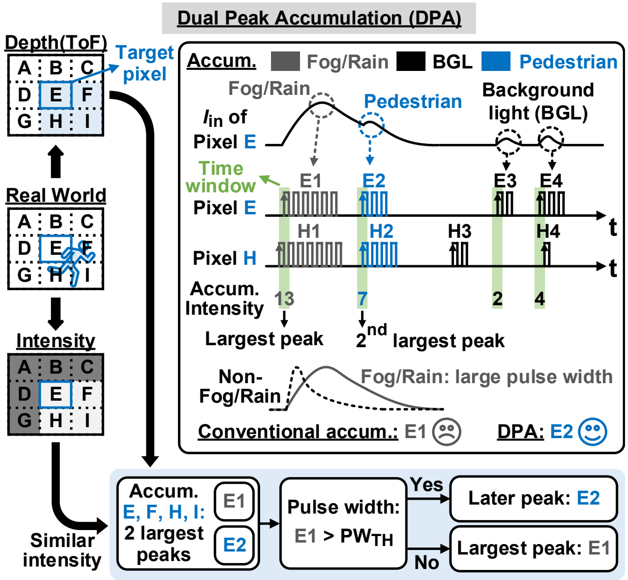

Fig. 5. Diagram and examples of the dual peak accumulation (DPA) algorithm for fog/rain removal.

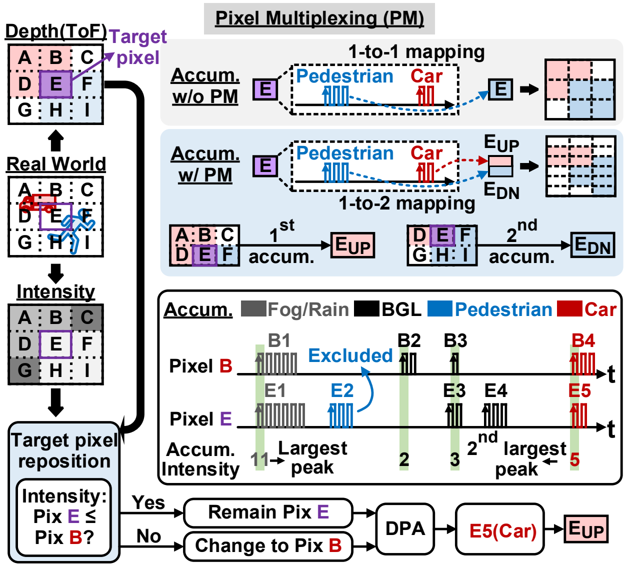

Fig. 6. Diagram and examples of pixel multiplexing (PM) algorithm for vertical super-resolution.

B. Dual-Peak Accumulation

Fig. 5 details the DPA algorithm. When LiDAR detects both fog/rain echoes (E1/H1) and target echoes (E2/H2), conventional accumulation algorithms [3-6] tend to retain only the peak value, resulting in misleading interference. The proposed DPA algorithm addresses this issue by preserving both the largest and the second-largest accumulated values. It then selects one based on the acquired pulse width to remove fog/rain, thereby enhancing the depth perception capabilities of LiDAR in adverse weather scenarios. If the acquired intensity exceeds the preset threshold, the algorithm selects the echo representing the farther target (E2) to aid fog/rain removal, since fog and rain generally appear in front of the target. Otherwise, the algorithm chooses the echo with the largest peak (E1) to prevent misidentifying a nearby target echo as interference. Moreover, the DPA algorithm improves the signal-to-background ratio for long-range imaging.

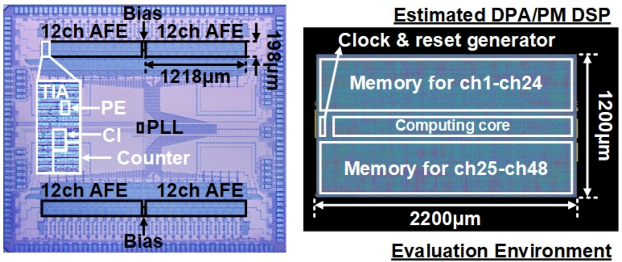

	Power [mW]
Bias	1.19
1GHz PLL	1.20
48× AFE	357.1
DSP	68.8
Total	428.3

Fig. 7. Die photo, estimated DSP, power breakdown, and LiDAR evaluation environment with artificial fog.

C. Pixel Multiplexing

Fig. 6 presents the PM algorithm, which is integrated into the DPA for super-resolution. Theoretically, each channel can receive echoes from all objects within its field of view. Conventional accumulation algorithms [3-6] create a 1-to-1 pixel correspondence between the resulting depth image and the pre-processed depth matrix, which may cause lower-intensity objects in a target pixel to be misinterpreted as noise and subsequently discarded. In contrast, the PM algorithm separately accumulates the target pixel (E) along with the adjacent pixels above and below it within a window, fully exploiting the multiple echoes present in the target pixel through two independent accumulations. The PM method achieves a 1-to-2 mapping (E-to-E_{UP}/E_{DN}), thus enhancing image resolution without increasing the number of channels and scans. Notably, the target pixel must be repositioned according to its intensity to avoid interference between high-intensity objects (E2) and low-intensity objects (E5) during accumulation. Suppose the intensity of the original target pixel (E) is higher than that of the pixels above (B) or below (H) it, the target pixel is repositioned to the corresponding adjacent pixel. Conversely, if the original intensity of the target pixel is equal to or lower than that of its neighbors, it remains unchanged.

III. Measurement Results

The prototype LiDAR chip is fabricated using a 65nm CMOS process, as shown in Fig. 7. It consumes 359.5mW, excluding the estimated 68.8mW from a DPA/PM-DSP. An artificial fog is generated with a fog simulator, with a visibility meter indicating its concentration. Fig. 8 shows the maximum measured distance achieved by the proposed fog/rain removal across various visibility conditions, while highlighting the 120m-visibility precision under power supply variations. Fig. 9 depicts the precision and accuracy results for a 10%-reflectivity target under 100klux of sunlight. The maximum fog-free detection range is 210m, reduced to 90m by artificial fog (120m visibility). However, the proposed fog/rain removal restores the detection range to 170m while presenting an uncalibrated precision of 31cm. Meanwhile, the distance error remains within 58cm, and a post-compensation method [8] reduces it to less than 1.5cm. Fig. 10 illustrates depth images captured under both fog-free

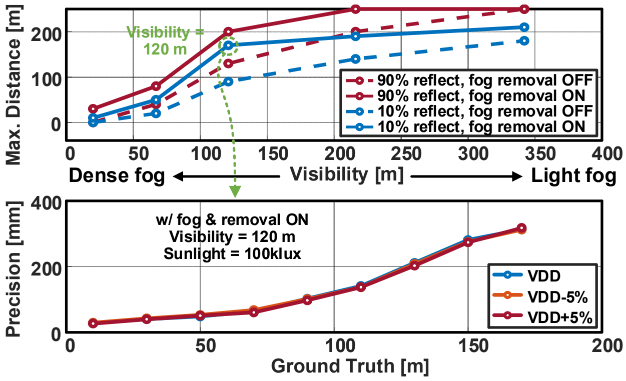

Fig. 8. Measured maximum distance under different fog concentrations (visibility) and the robustness verification of LiDAR.

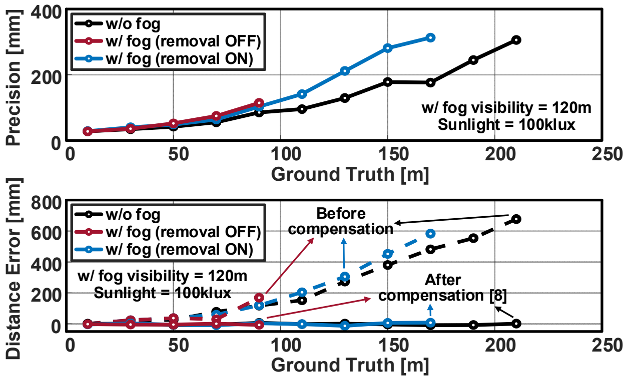

Fig. 9. Measured precision and distance error under fog-free, foggy (removal OFF), and foggy (removal ON) conditions at 100klux.

and foggy conditions at 100klux. The proposed removal method significantly improves the depth imaging quality in foggy scenarios. Table I compares the prototype with the state-of-the-art LiDARs. It achieves a competitive fps with improved detection distance in adverse weather conditions.

IV. Conclusion

This paper enhances LiDAR performance in adverse weather conditions by utilizing the PE-TIA for fog/rain extraction and the DPA for removal. Additionally, the PM technique supports mapping from a single AFE channel to two pixels, facilitating 2× vertical pixel super-resolution. The prototype LiDAR extends the 10%-reflectivity detection distance from 90m to 170m under a 120m-visibility artificial fog scenario, while the 48× AFEs provide an imaging resolution of 512×96 at 50fps using line-scanning.

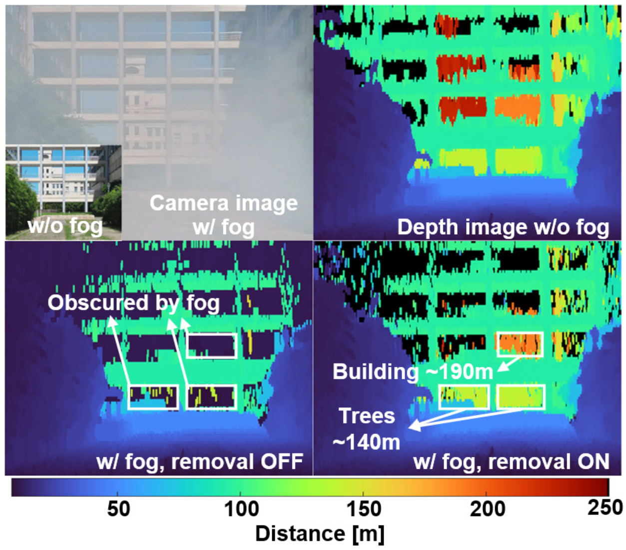

Fig. 10. Measured depth images under fog-free, foggy (removal OFF), and foggy (removal ON) conditions at 100klux.

TABLE I. Comparison with State-of-the-Art LiDARs

Parameter	This work	VLSI 2025 [9]	JSSC 2024 [6]	ISSCC 2021 [10]	ISSCC 2020 [4]	ISSCC 2018 [5]
Process	65nm	90nm 40nm	65nm	90nm 40nm	28nm	28nm
Photodetector	Off-chip SiPM	On-chip SPAD	Off-chip SiPM	On-chip SPAD	Off-chip SiPM	Off-chip SiPM
Scanning Mode	1D	1D	2D	1D	2D	2D
Channel	48	N/A	8	N/A	40	20
Field of View	20°×15°	120°×26°	20°×7.5°	25.2°×9.5°	N/A	N/A
Pixel Resolution	512×96	2400×520	256×192	168 x 63	240×192	240×96
Frame Rate	50fps	20fps	30fps	20fps	10fps	10fps
Background Light	100klux	120klux	50klux	117klux	70klux	70klux
Max. Distance	210-250m	300m	160-240m	150-200m	225m	200m
Depth Precision	0.14%	0.03%	0.10%	N/A	0.25%	0.13%
Fog/Rain Removal	Yes	No	No	No	No	No
Max. Distance w/ Fog	170m	N/A	N/A	N/A	N/A	N/A
AFE Power /Ch	7.44mW	N/A	7.84mW	N/A	10mW	39mW

References

[1] Toshiba Corporation. (2023). *Toshiba Develops World's First LiDAR with 99.9% Tracking Accuracy*. [Online] Available: https://www.global.toshiba/ww/technology/corporate/rdc/rd/topics/23/2309-02.html

[2] K. Qian, S. Zhu, X. Zhang, and L. E. Li, "Robust multimodal vehicle detection in foggy weather using complementary LiDAR and radar signals," in 2021 *IEEE/CVF Conference on Computer Vision and Pattern Recognition (CVPR)*, Nov. 2021, pp. 444-453.

[3] C. Niclass, et al., "A 0.18-µm CMOS SoC for a 100-m-range 10-frame/s 200×96-pixel time-of-flight depth sensor," *IEEE Journal of Solid-State Circuits*, vol. 49, no. 1, pp. 315-330, Jan. 2014.

[4] S. Kondo, et al., "A 240×192-pixel 10fps 70klux 225m-range automotive LiDAR SoC using a 40ch 0.0036 mm^2 voltage/time dual-data-converter-based AFE," in *IEEE Int. Solid-State Circuits Conf. (ISSCC)*, Feb. 2020, pp. 94-95.

[5] K. Yoshioka, et al., "A 20ch TDC/ADC hybrid SoC for 240×96-pixel 10%-reflection <0.125%-precision 200m-range imaging LiDAR with smart accumulation technique," in *IEEE Int. Solid-State Circuits Conf. (ISSCC)*, Feb. 2018, pp. 92-93.

[6] C. Zou, Y. Ou, Y. Zhu, R. P. Martins, C.-H. Chan, and M. Zhang, "A 256 × 192-pixel direct time-of-flight LiDAR receiver with a current-integrating-based AFE supporting 240-m-range imaging," *IEEE Journal of Solid-State Circuits*, vol. 59, no. 11, pp. 3525-3537, Nov. 2024.

[7] Z. Liu, C. Chye Boon, and Y. Dong, "A 0.6 V, 1.74 mW, 2.9 dB NF inductorless wideband LNA in 28-nm CMOS exploiting noise cancellation and current reuse," *IEEE Transactions on Circuits and Systems I: Regular Papers*, vol. 71, no. 8, pp. 3561-3572, Aug. 2024.

[8] G. M. Williams. (2021). *Range-Walk Correction Using Time Over Threshold*. [Online]. Available: https://www.allegromicro.com/en/insights-and-innovations/technical-documents/p0179-tot-range-walk-correction

[9] T. Yui et al., "A 25M points/s back-illuminated stacked SPAD direct time-of-flight depth sensor with equivalent time sampling for automotive LiDAR," in *2025 Symposium on VLSI Technology and Circuits (VLSI Technology and Circuits)*, July 2025, pp. 1-3.

[10] O. Kumagai, et al., "A 189×600 back-illuminated stacked SPAD direct time-of-flight depth sensor for automotive LiDAR systems," in *IEEE Int. Solid-State Circuits Conf. (ISSCC)*, Feb. 2021, pp. 110-111.